Journal of Magnetism and Magnetic Materials 497 (2020) 165970

Contents lists available at ScienceDirect

Journal of Magnetism and Magnetic Materials

journal homepage: www.elsevier.com/locate/jmmm

Research articles

Room temperature ferromagnetism from magnetic ion free binary oxide film

Jiwoong Kim[a], Sehwan Song[a], Yesul Choi[a], Dooyong Lee[a], Hyegyeong Kim[b], Ho-Sun Lee[b], Jong-Seong Bae[c], Sungkyun Park[a,b,c,*]

[a] Department of Physics, Pusan National University, Busan 46241, Republic of Korea
[b] Core Research Facilities, Pusan National University, Busan 46241, Republic of Korea
[c] Busan Center, Korea Basic Science Institute, Busan 46742, Republic of Korea

ARTICLE INFO

Keywords:
SnO_2
Oxygen vacancies
Room temperature ferromagnetism

ABSTRACT

We herein investigated the magnetic moment of thickness-dependent SnO_2 films at room temperature. The saturation magnetization of SnO_2 films grown on the r-plane sapphire substrate was decreased with increasing the film thickness. An areal saturation magnetization, a magnetic moment in the unit surface area, did not vary with increasing film thickness. Hall effect measurement indicated that the charge carrier from oxygen vacancy was presented in the epitaxial SnO_2 films. Furthermore, X-ray photoelectron spectroscopy analysis revealed that the oxygen vacancy profiles were consistent with that of magnetization. These results suggest that oxygen vacancies at the surface region are the source of the magnetic moment in SnO_2 films.

1. Introduction

Room-temperature ferromagnetism of dilute magnetic semiconducting oxides has seen considerable interest for application in spin-based semiconducting devices [1,2]. However, the origin of ferromagnetism in these materials, such as SnO_2, CeO_2, HfO_2, ZnO, is still a mystery, as there are no unpaired electrons in the *d*-state. Recently, defects have been reported to be the essential components affecting the magnetic characteristics in the d^0-ferromagnetism [3–6]. For example, the oxygen vacancy is responsible for the ferromagnetic characteristics because the spin-polarized state is expected to be developed from the defect in various oxide systems [4,5]. Likewise, the characteristics of defects, including oxygen vacancies, cation vacancies, and interstitials, have been intensively studied to understand the physical mechanisms associated with dilute magnetic oxides [7].

In contrast, the role played by defects in the magnetic characteristics of the SnO_2 system is still controversial. First, a density functional theory (DFT) calculation showed that an Sn vacancy could result in a ferromagnetic moment as high as 4.00 μ_B, while a neutral oxygen vacancy did not induce any magnetic moment [8]. However, it is difficult to accept that an Sn vacancy is the source of ferromagnetism because of its high formation energy [9]. Moreover, various experimental works showed the reduced magnetic moment in SnO_2 after annealing in an oxygen environment, resulting in the oxygen vacancy was the source of ferromagnetism [3,10–12]. Nevertheless, several DFT calculations presented that the oxygen vacancy was still nonmagnetic [8,13,14].

Recently, it is suggested that the singly charged oxygen vacancy (V_O^+) resided at the boundary might be the origin of magnetism in the SnO_2 system from DFT calculation. Wang et al. showed that the V_O^+ could create a spin-split state in manipulated bandgap at the boundaries [13]. In addition, Apostolov et al. calculated the magnetization of SnO_2 nanoparticle based on spin-phonon interaction, which showed the magnetization decreased with increasing particle size [14]. According to these observations, the enhanced magnetization in a smaller volume of both SnO_2 powder and film [10,15] is expected to reveal the surface magnetism induced by the oxygen vacancy. Furthermore, Chang et al. suggested that localized carriers at the surface from defects, such as oxygen or cation vacancies, have magnetic triplet states as a form of p_z-state, calculated by the image charge method [10]. Therefore, it is essential to discover the direct evidence to verify the surface magnetic state of SnO_2.

In this paper, we report the induced surface ferromagnetism of undoped SnO_2 at room temperature. The consistent areal magnetization of epitaxial SnO_2 film regardless of film thickness supports that the magnetic moment resides at the surface, which cannot be formed at the interface between SnO_2 and Al_2O_3 substrate. From a careful analysis of spectroscopic data, we find that the oxygen vacancy profile of the film is consistent with the magnetic profile of the film, resulting in that oxygen vacancies play the primary role in room-temperature ferromagnetism.

* Corresponding author at: Department of Physics, Pusan National University, Busan 46241, Republic of Korea.
E-mail address: psk@pusan.ac.kr (S. Park).

https://doi.org/10.1016/j.jmmm.2019.165970
Received 6 August 2019; Received in revised form 23 September 2019; Accepted 8 October 2019
Available online 09 October 2019
0304-8853/

2. Material and methods

From a 2-inch SnO_2 target (99.99%, LTS Research Laboratories, Inc.), SnO_2 films were grown on an Al_2O_3 $(10\bar{1}2)$ substrate using a radio frequency magnetron sputtering system. After evacuating the vacuum chamber lower than 1.0×10^{-6} mTorr, the pressure was kept at 30 mTorr by flowing Ar gas (25 SCCM). Films were fabricated by varying the deposition time (15, 30, 60, 120, and 180 s) at a substrate temperature of 700 °C. Room-temperature ferromagnetic properties were confirmed using vibrating sample magnetometry mode (the frequency is 12.8 Hz, traveling distance is 6 mm, and averaging time is 15 s) in a superconducting quantum interference device (SQUID; MPMS-3, Quantum Design) at the Core Research Facilities at Pusan National University, Busan, Korea. The thickness and structural properties of the films were examined by using a diffractometer with a monochromated Cu Kα (λ = 1.5406 Å) X-ray source at the Korea Basic Science Institute (Empyrean, PANalytical), Daejeon, Korea. The carrier concentration and electrical resistivity of the films were determined by Hall effect measurements with van der Pauw geometry [16] under a magnetic field of 0.75 T at room temperature. The chemical states of the surface of SnO_2 films were investigated by X-ray photoelectron spectroscopy (XPS) by using a monochromated Al *Kα* ($h\nu$ = 1486.6 eV) source at the Core Research Facilities at Pusan National University (AXIS Supra, Kratos Analysis), Busan, Korea. The binding energy of the spectra was calibrated using the binding energy of C–C bonding in the C 1*s* core-level X-ray photoelectron spectra (284.5 eV) [17]. Finally, the possible magnetic impurities (Fe, Co, Ni) were examined for the selected films using a high-resolution inductively coupled plasma mass spectrometer (ICP-MS) & laser ablation microprobe system (J200, Applied Spectra) at the Core Research Facilities at Pusan National University, Busan, Korea.

3. Results and discussion

The magnetic hysteresis loops of SnO_2 films with various thicknesses at 300 K are shown in Fig. 1(a). The magnetization was acquired by properly subtracting the diamagnetic signal from the Al_2O_3 substrate with consideration of the volume of each film, calculated from the surface area, and the film thickness, determined by X-ray reflectivity (Fig. S1) [18]. Notably, all of the films showed ferromagnetic properties at room temperature. Furthermore, the saturation magnetization (M_S) of SnO_2 films decreased with increasing film thickness (Fig. 1(b)). Similar results of M_S variations depending on the volume of SnO_2 were observed. The magnetic moment was enhanced in the thinner SnO_2 film [10]. The areal magnetizations (M_S·t) of SnO_2 films are independent of the film thickness (Fig. 1(c)), indicating the magnetization is not uniformly distributed in the vertical direction of the film, although a wide difference of the areal magnetization was noticed from others [10].

The possible presence of magnetic impurities such as Fe, Co, and Ni, affecting the ferromagnetic signal was examined. From a survey scan of XPS measurements (Fig. S3), there are no components except for Sn, O, and C in the SnO_2 films. However, for the 3.8- and 7.3-nm-thick films, Al 2*p* spectra, which originate from the Al_2O_3 substrate, were observed (Fig. S4(a)) because the film thickness is thinner than the X-ray probing depth [19]. In addition, ICP-MS measurement confirms the absence of noticeable impurities at the ppm-level, demonstrating that the effect of magnetic impurities on the measured magnetic moment is negligible (Table S1).

The structural characteristics from the XRD measurements of SnO_2 films depending on the film thickness are shown in Fig. 2. Rutile SnO_2 (tetragonal; $P4_2/mnm$) was epitaxially grown in the (1 0 1) orientation without a secondary phase. As the film thickness increases, the decrease and increase of the full width at half maximum (FWHM) and the peak intensity are observed, respectively (Table 1). Two consecutive SnO_2 (1 1 0) peaks in the azimuthal plane (Fig. S2) show an angle difference of 100°, while each peak is 50° apart with respect to the Al_2O_3 (0006) peak. These results indicate that all of the SnO_2 films deposited on the Al_2O_3 substrate have a following structural relationship of $SnO_2(1\,0\,1)[0\,1\,0]||Al_2O_3(10\bar{1}2)[\bar{1}210]$ [20]. It was demonstrated that in the epitaxial SnO_2 (1 0 1) film on the substrate there are crystallographic shear planes (CSPs), called as antiphase boundary (APB), created by a difference between lattice mismatches in the plane (11.45% along the SnO_2 $[\bar{1}01]$ direction, whereas −0.42% along SnO_2 [1 0 1] direction) [20,21]. Hong et al. found that a metal cluster affecting the magnetic properties was precipitated at the interface between transition metal-doped SnO_2 film and Al_2O_3 $(10\bar{1}2)$ substrate owing to the lattice mismatch [22–24]. However, because of the lack of magnetic impurities, we expect that there were no magnetic clusters precipitated at the interface. In addition, the strain state of SnO_2 films is negligible because the values of the peak position are close to that of the bulk (2θ = 33.89°, ICSD #16635), expecting the existence the CSPs to release the interfacial misfit strain [25].

The crystallite size along the normal direction was investigated using the FWHM of SnO_2 (1 0 1) peaks by employing the Scherrer equation [26] (Table 1). For the 3.8-nm-thick film, the crystallite size is comparable to the film thickness. However, the difference between the crystallite size and film thickness becomes larger with increasing film thickness. According to the dynamic theory of X-ray diffraction, the crystallite size is identical to that of a single crystal up to 600 nm, if the material has the linear absorption coefficient below 2117.3 cm^{-1}, corresponding to CeO_2 [27], even though the exact size is limited by the extrinsic bandwidth of the diffractometer [28]. Considering that the absorption coefficient of SnO_2 is 1385.7 cm^{-1} at 8.0 keV (near the energy of Cu Kα radiation) [29], the increased difference between

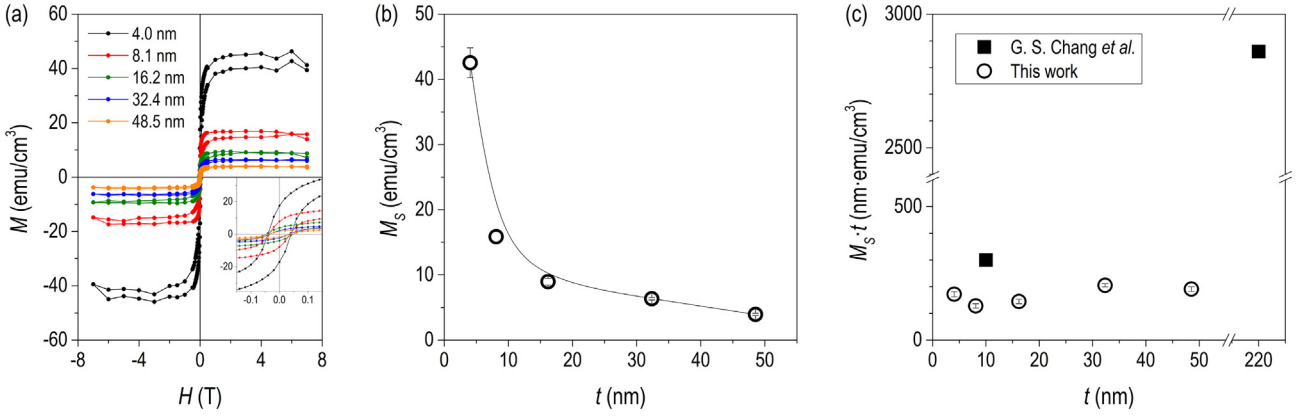

Fig. 1. (a) Room temperature magnetic hysteresis loops of SnO_2 films with various thicknesses. Thickness-dependent (b) saturation magnetization (M_S) and (c) surface magnetization of the SnO_2 films. Inset in Fig. 1(a) shows enlarged magnetic hysteresis loops for the films.

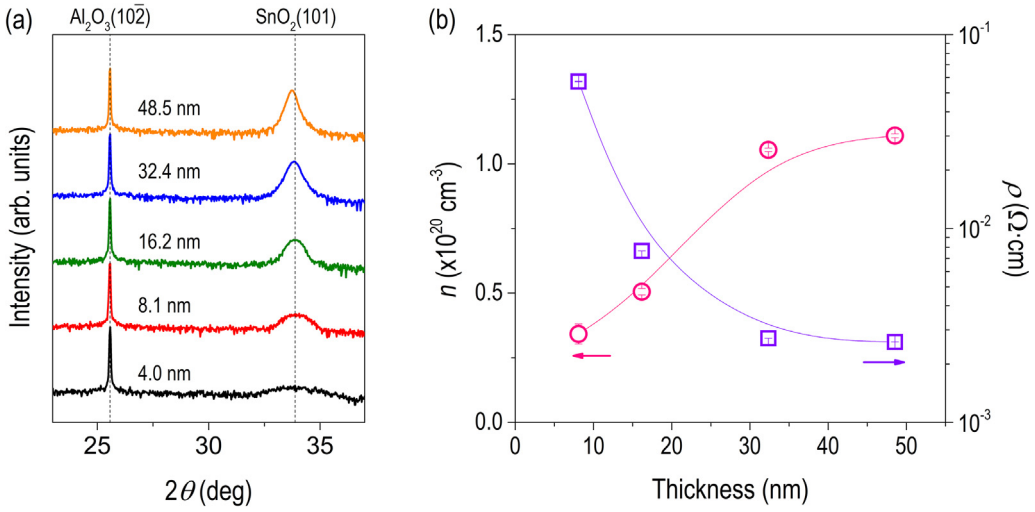

Fig. 2. Film thickness-dependent (a) normal X-ray diffraction profiles and (b) carrier concentration and resistivity of SnO_2 films. Vertical dotted lines in Fig. 2(a) indicate reference peak positions of SnO_2 (ICSD #16635) and Al_2O_3 (ICSD #73076).

Table 1
Peak positions and FWHMs of SnO_2 (1 0 1) peak, and crystallite sizes of various SnO_2 film thicknesses.

Film thickness, *t* (nm)	Peak position (deg.)	FWHM (deg.)	Crystallite size (nm)
3.8	33.78 ± 0.03	2.38 ± 0.11	3.45 ± 0.25
7.3	33.92 ± 0.01	1.19 ± 0.04	6.90 ± 0.45
16.5	33.87 ± 0.01	0.72 ± 0.01	11.41 ± 0.66
29.8	33.83 ± 0.01	0.51 ± 0.01	16.10 ± 0.96
42.7	33.74 ± 0.01	0.36 ± 0.01	23.80 ± 1.43

crystallite size and film thickness as the film thickness increased is associated with decreasing crystallinity of the films with larger thickness. In other words, the highly crystalline SnO_2 is formed at the bottom interface and limited when the film thickness increases. Since the density of CSP is the highest at the interface [25], this observation indicates that CSPs terminated inside SnO_2 film improve the crystallinity at the interface.

The electrical resistivity in SnO_2 films determined by Hall effect measurements is shown in Fig. 2(b). All of the films, except for the thinnest film, exhibited *n*-type characteristics, representing an oxygen vacancy could be presented as a donor in the SnO_2 films. The carrier concentration (resistivity) decreased (increased) with decreasing film thickness. Notably, J. E. Dominguez et al. examined that density of CSPs decreased with increasing thickness of SnO_2(1 0 1) film while partial dislocations were increased [25]. According to these results, the more carriers were trapped at CSPs in the thinner film. Notably, it is deduced that the measured dc-electrical resistivity is affected by scattering from CSPs, and the highest resistance is shown at the thinnest film, which is higher than instrument limitation.

Based on the hypothesis of the oxygen vacancy-induced surface ferromagnetic ordering of SnO_2 films [10,15], the relative content of oxygen vacancies at the film surface was examined using O 1*s* core-level X-ray photoelectron spectra. Prior to analyzing the chemical state of oxygen, the state of Sn was confirmed to be mostly composed of the Sn^{4+} state (Fig. S4(b)). The binding energy of electrons in the O 1*s* state influenced by oxygen vacancies is higher than that of lattice oxygen because the effective nuclear charge (Z_{eff}) at the nearest-neighbor O^{2-} ion for the oxygen vacancy is increased by a reduced screening of the electrons in the ion [24]. Fig. 3(a) shows the film thickness-dependent O 1*s* core-level X-ray photoelectron spectra. The spectra were deconvoluted in three distinct oxidation states, including oxygen in the SnO_2 crystal structure (O-Sn, 530.3 eV [30]), oxygen vacancies (V_O, 531.4 eV [31]), and adventitious carbon caused by surface contamination (O-C, 532.0 eV [32]). The relative oxygen vacancy contents were evaluated by the relative peak areal intensity ratio concerning lattice oxygen $\left(\frac{A(V_O)}{A(O-Sn)+A(V_O)} \times 100(\%)\right)$, as shown in Fig. 3(b). The larger content of oxygen vacancies (~17%) was originated by the high-power and high-temperature sputtering process. The higher sputter power generates the more V_O due to energy transfer from accelerated ionized Ar gas [33]. Furthermore, the thermal energy assists in introducing the V_O in the oxide film if the oxygen partial pressure is low enough [34,35]. The V_O can be eliminated by introducing oxygen gas in the film growth or post-annealing process under an oxygen environment [10,11]. However, the relative content of oxygen vacancies is consistent, regardless of the film thickness, except for the thinnest one (i.e., the 3.8-nm-thick film). Regarding the substrate effect in the 3.8-nm-thick film, which is negligible for the 7.3-nm-thick film, the area of V_O should be integrated with the oxygen (or oxygen vacancies) in Al_2O_3 (531.3 eV [36]). Therefore, the V_O content of the thinnest SnO_2 film shown in Fig. 3(b) was overestimated [20]. Therefore, the amount of oxygen vacancy at the surface is consistent regardless of the film thickness.

As a result, uniform oxygen vacancy formation is consistent with uniform areal magnetization for SnO_2 films regardless of film thickness, suggesting that the oxygen vacancy at the surface is the origin of ferromagnetism. This result can be supported by the magnetic moment from V_O^+ at the surface in which band structure is modified [13]. From angle-resolved XPS measurement, it has been found that surface band bending is occurred in SnO_2(1 0 1) film due to surface electron accumulation [37–39]. Since we assume that there is no oxygen vacancy at the interface due to the formation of CPSs [20], we expect that the magnetic moment was resided at the surface due to the spin-split impurity band. On the other hand, according to theoretical results from image charge method [10] and spin-phonon interaction [14], the modified band structure is unnecessary to induce the magnetic moment at the surface. In this regard, the magnetic ground state of the defect at the surface is needed to verify to understand the d^0-ferromagnetism in binary oxide films.

4. Conclusion

The room-temperature ferromagnetism of undoped SnO_2 films with varying film thickness was investigated. The unusual room-temperature ferromagnetism decreased with increasing film thickness. However, the areal magnetization was uniform regardless of film thickness, unlike other observations. All the films showed SnO_2(1 0 1)

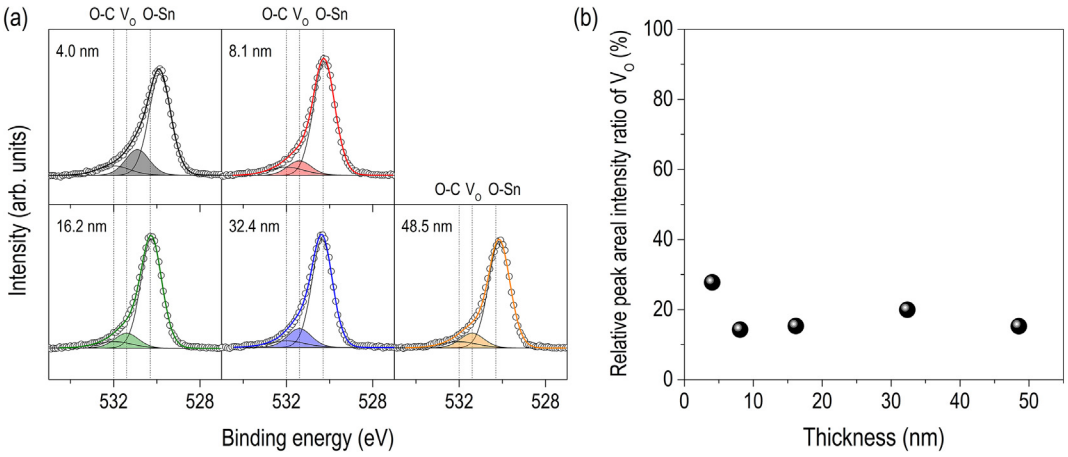

Fig. 3. (a) O 1*s* core-level X-ray photoelectron spectra of thickness-dependent SnO_2 films. Vertical dotted lines indicate oxygen in the SnO_2 crystal structure (O-Sn [30]), oxygen vacancies (V_O [31]), and adventitious carbon from surface contamination (O-C [32]). (b) Relative peak areal intensity ratio of V_O with respect to O-Sn as a function of thickness.

$[0\,1\,0]||Al_2O_3(10\bar{1}2)[\bar{1}2\bar{1}0]$ epitaxial relationships, representing films possess crystallographic defects (CSPs) by the lattice mismatch. From Hall effect measurement, the increment of *n*-type carrier concentration with respect to film thickness displayed that oxygen vacancies acted as a donor. XPS measurements showed that the relative amount of oxygen vacancies with respect to lattice oxygen was also the same for all the films, which is consistent with the film thickness-dependent magnetization profile. These results provide evidence of induced surface magnetization by oxygen vacancies in SnO_2 films.

Declaration of Competing Interest

The authors declare that they have no known competing financial interests or personal relationships that could have appeared to influence the work reported in this paper.

Acknowledgments

This study is supported in part by NRF-Korea (2017K1A3A7A09016305 and 2018R1D1A1B07045663) and a KBSI grant (C38529) to S. Park. J. Kim also funded in part by NRF-Korea (2015H1A2A1034200).

Appendix A. Supplementary data

Supplementary data to this article can be found online at https://doi.org/10.1016/j.jmmm.2019.165970.

References

[1] W.Y. Choi, H.-J. Kim, J. Chang, S.H. Han, A. Abbout, H.B.M. Saidaoui, A. Manchon, K.-J. Lee, H.C. Koo, Nano Lett. 18 (2018) 7998–8002.
[2] H. Ohno, Science 281 (1998) 951.
[3] A. Sundaresan, R. Bhargavi, N. Rangarajan, U. Siddesh, C.N.R. Rao, Phys. Rev. B 74 (2006) 161306.
[4] V.K. Paidi, D.L. Brewe, J.W. Freeland, C.A. Roberts, J. van Lierop, Phys. Rev. B 99 (2019) 180403.
[5] M. Venkatesan, C.B. Fitzgerald, J.M.D. Coey, Nature 430 (2004) 630-630.
[6] S. Mal, S. Nori, J. Narayan, J.T. Prater, D.K. Avasthi, Acta Mater. 61 (2013) 2763–2768.
[7] J.M.D. Coey, Nat. Mater. 18 (2019) 652–656.
[8] G. Rahman, V.M. García-Suárez, S.C. Hong, Phys. Rev. B 78 (2008) 184404.
[9] Ç. Kılıç, A. Zunger, Phys. Rev. Lett. 88 (2002) 095501.
[10] G.S. Chang, J. Forrest, E.Z. Kurmaev, A.N. Morozovska, M.D. Glinchuk, J.A. McLeod, A. Moewes, T.P. Surkova, N.H. Hong, Phys. Rev. B 85 (2012) 165319.
[11] L. Zhang, S. Ge, Y. Zuo, B. Zhang, L. Xi, J. Phys. Chem. C 114 (2010) 7541–7547.
[12] J. Li, G. Bai, Y. Jiang, Y. Du, C. Wu, M. Yan, J. Magn. Magn. Mater. 426 (2017) 545–549.
[13] H. Wang, Y. Yan, K. Li, X. Du, Z. Lan, H. Jin, Phys. Status Solidi B 247 (2010) 444–448.
[14] A.T. Apostolov, I.N. Apostolova, S. Trimper, J.M. Wesselinowa, Mod. Phys. Lett. B 31 (2017) 1750351.
[15] S. Shi, D. Gao, Q. Xu, Z. Yang, D. Xue, RSC Adv. 4 (2014) 45467–45472.
[16] L.J. van der Pauw, Semiconductor Devices: Pioneering Papers, World Sci. (1991) 174.
[17] J.F. Moulder, J. Chastain, Handbook of X-ray Photoelectron Spectroscopy: A Reference Book of Standard Spectra for Identification and Interpretation of XPS Data, Physical Electronics Division, Perkin-Elmer Corp, Eden Prairie, MN, 1992.
[18] R. Ranchal, B.S. Yadav, A. Trampert, J. Phys. D: Appl. Phys. 46 (2013) 075003.
[19] M. Oshima, Chapter 8 - Nanolayer Analysis by Photoelectron Spectroscopy, in: T. Imae (Ed.), Nanolayer Research, Elsevier, Amsterdam, 2017, pp. 285–333.
[20] J.E. Dominguez, X.Q. Pan, L. Fu, P.A. Van Rompay, Z. Zhang, J.A. Nees, P.P. Pronko, J. Appl. Phys. 91 (2002) 1060–1065.
[21] H. Mun, H. Yang, J. Park, C. Ju, K. Char, Appl. Mater. 3 (2015) 076107.
[22] N.H. Hong, J. Sakai, W. Prellier, A. Hassini, J. Phys. Condensed Matter 17 (2005) 1697–1702.
[23] N.H. Hong, J. Sakai, Phys. B: Condensed Matter 358 (2005) 265–268.
[24] N.H. Hong, A. Ruyter, W. Prellier, J. Sakai, N.T. Huong, J. Phys. Condensed Matter 17 (2005) 6533–6538.
[25] J.E. Dominguez, L. Fu, X.Q. Pan, Appl. Phys. Lett. 81 (2002) 5168–5170.
[26] J.I. Langford, A.J.C. Wilson, J. Appl. Crystallogr. 11 (1978) 102–113.
[27] F.T.L. Muniz, M.A.R. Miranda, C. Morilla dos Santos, J.M. Sasaki, Acta Crystallogr. Sec. A 72 (2016) 385–390.
[28] B.D. Cullity, S.R. Stock, Elements of X-ray Diffraction, third ed., Prentice Hall, Upper Saddle River, NJ, 2001.
[29] J.H. Hubbell, S.M. Seltzer, X-Ray Mass Attenuation Coefficients, National Institute of Standards and Technology, Gaithersburg, MD, 2004.
[30] R.O. Ansell, T. Dickinson, A.F. Povey, P.M.A. Sherwood, J. Electron Spectros. Relat. Phenomena 11 (1977) 301–313.
[31] J.C.C. Fan, J.B. Goodenough, J. Appl. Phys. 48 (1977) 3524–3531.
[32] Y. Wen, H. Ding, Y. Shan, Nanoscale 3 (2011) 4411–4417.
[33] W.-F. Wu, B.-S. Chiou, S.-T. Hsieh, Semicond. Sci. Technol. 9 (1994) 1242–1249.
[34] H.-W. Lee, W.-J. Cho, AIP Adv. 8 (2018) 015007.
[35] K. Wang, Y. Chang, L. Lv, Y. Long, Appl. Surf. Sci. 351 (2015) 164–168.
[36] A.M. Venezia, R. Bertoncello, G. Deganello, Surf. Interface Anal. 23 (1995) 239–247.
[37] S.K. Vasheghani Farahani, T.D. Veal, J.J. Mudd, D.O. Scanlon, G.W. Watson, O. Bierwagen, M.E. White, J.S. Speck, C.F. McConville, Phys. Rev. B 90 (2014) 155413.
[38] T. Nagata, O. Bierwagen, M.E. White, M.Y. Tsai, Y. Yamashita, H. Yoshikawa, N. Ohashi, K. Kobayashi, T. Chikyow, J.S. Speck, Appl. Phys. Lett. 98 (2011) 232107.
[39] T. Nagata, O. Bierwagen, Z. Galazka, S. Ueda, M. Imura, Y. Yamashita, T. Chikyow, Jpn. J. Appl. Phys. 58 (2019) 080903.